https://doi.org/10.5194/egusphere-2026-3930
Preprint. Discussion started: 14 July 2026

Diurnal heating of the lower atmosphere over land determines the Vapor Pressure Deficit (VPD)

Sarosh Alam Ghausi[1,2], Tejasvi Ashish Chauhan[2] and Axel Kleidon[2]

[1] Kotak School of Sustainability, Indian Institute of Technology Kanpur, 208016, India.
[2] Biospheric Theory and Modelling Group, Max Planck Institute for Biogeochemistry, Jena 07745, Germany.

Correspondence to: Sarosh Alam Ghausi (saroshag@iitk.ac.in)

Abstract. The Vapor Pressure Deficit (VPD) is a key climatological variable that relates to atmospheric dryness, vegetation productivity and terrestrial water and carbon fluxes. It is often interpreted to be a direct reflection of the atmospheric moistening by land evaporation, or its absence, and hypothesized to play a central role in land-atmosphere interactions. Here, we show that a large part of VPD results from the diurnal heating of the lower atmosphere, so that it is tightly linked to the Diurnal Air Temperature Range (DTR). We use an analytical expression for DTR that mechanistically links it to changes in the heat content of the lower atmosphere, which we then use to estimate VPD using the slope of the saturation vapor pressure curve. When applied across continents, our approach reproduces observed spatial and temporal variability in VPD with R^2 of 0.9 and 0.8 respectively. It captures observed responses of VPD to solar radiation, clouds, and soil water stress across diverse climate and moisture regimes. It also explains the characteristic hump-shaped relationship between evaporation and VPD as an emergent consequence of changes in DTR during transition from energy- to water-limited conditions. Our findings suggest that much of the observed VPD variability and its responses can be explained by the thermodynamic controls on lower-atmospheric heating, rather than moistening. This explanation of VPD variations implies that VPD largely responds to land surface energy partitioning, with important implications for interpreting VPD-ecosystem relationships, land-atmosphere feedbacks and evaluating aridity trends under global warming.

https://doi.org/10.5194/egusphere-2026-3930
Preprint. Discussion started: 14 July 2026

1 Introduction

The Vapor Pressure Deficit (VPD), defined as the difference between saturation and the actual vapor pressure in the air near the surface, is a key variable for land surface climate. It directly relates to the relative humidity of the near-surface air (with rh = 1 - VPD/esat) and, hence, atmospheric dryness. VPD serves as a widely used metric to estimate atmospheric evaporative demand, with higher VPD implying higher evaporation rates because of a greater gradient in vapor pressure between leaves and soils and the atmosphere (Allen et al 1998). It thereby has been argued to be central in shaping terrestrial water and carbon exchanges (Gentine et al., 2019), affecting vegetation productivity (Yuan et al., 2019; Zhong et al., 2023), modulating plant physiological responses (Franks et al., 1997; Medlyn et al., 2011; Grossiord et al., 2020), and being a key variable involved in land-atmosphere feedbacks that can exacerbate climate extremes and aridity trends (Sherwood & Fu, 2014; Fang et al., 2022; Zhang et al., 2024; Novick et al., 2024).

Despite its wide significance, interpreting VPD dynamics appears to be complicated by its close coupling with antecedent land-surface and, radiative conditions as well as their complex interactions. Not accounting for this coupling leads to overestimation of climate-driven ET increases (Zhou & Yu, 2025), contrasting projections of aridity (Huang et al., 2016; Berg & McColl, 2021), misattribution of ecosystem productivity to atmospheric and land-surface drivers (Liu et al., 2020; Lu et al., 2022; Fu et al., 2022) and confounding interpretations of evapotranspiration parameterizations (Novick et al., 2016; Buckley 2019; Vargas Zeppetello et al., 2023). As a result, disentangling the influence of VPD from antecedent soil-moisture and atmospheric conditions remains a central challenge, and the extent to which VPD independently modulates land–atmosphere exchange remains unclear.

Here, we take a simpler approach and show that much of the variability of VPD can be explained directly by the variability in diurnal air temperature range (DTR), which in turn can be understood as a consequence of surface heating by solar radiation and reduced evaporation (the effect of soil water stress) (Fig. 1). The physical mechanism is simple. During the day, solar radiation heats the surface, while net emission of longwave radiation, the sensible and latent heat flux cool the surface. While the first two cooling terms act to heat the lower atmosphere, the energy involved in the latent heat flux goes into water vapor, which does not heat the lower atmosphere unless it condenses. This heating from the surface is associated with a temperature increase in the convective boundary layer, which results in the variation of temperature that is reflected in the diurnal temperature range (DTR). In Ghausi et al. (2025), we showed that this approach, using the energy balances of the surface and the lower atmosphere, can describe the observed variations and trends of DTR very well.

Here, we extend this approach of Ghausi et al. (2025) to daily maximum VPD, which characterizes peak daytime atmospheric dryness. If we assume that the moisture content of the convective boundary layer remains mostly unchanged throughout the

https://doi.org/10.5194/egusphere-2026-3930
Preprint. Discussion started: 14 July 2026

day, then the heating from the surface and the warming of the air acts to increase the saturation vapor pressure. Since VPD is defined as esat - ea, with the actual vapor pressure ea assumed to stay fixed but esat increases according to Clausius-Clapeyron, we would then expect that the diurnal increase of VPD is directly proportional to DTR, with the proportionality given by the slope of the saturation vapor pressure curve, s = desat/dT. Hence, most of the variation in VPD should directly relate to the drivers of DTR, and modulated by the slope s.

We evaluate our explanation with respect to two major influences on VPD that are the major forcings for the DTR (as in Ghausi et al., 2025): (i) Absorbed solar radiation at the surface, Rs, which is modulated by clouds and seasonal variations; (ii) Soil water stress, that is, a reduction in the latent heat flux LE from its unstressed, potential value, as this additionally heats the lower atmosphere.

We test these influences with observations using global gridded datasets. With these influences, we can then understand why evaporation does not necessarily increase with VPD, but may in fact reduce under certain conditions, resulting in a non-linear hump-shaped curve, which has been reported previously (Zhang et al., 2014; Massmann et al., 2019; Grossiord et al., 2020). We show that this hump-shaped relationship between evaporation and VPD can be explained by how the atmospheric heat storage and DTR are modulated under water and energy limited evaporative conditions (Koster et al., 2009; Seneviratne et al., 2010).

We structure our paper as follows. To evaluate our interpretation, we first describe our methodology in which we decompose VPD into a minimum value and its diurnal variation, which we relate to the DTR. The DTR we then relate to solar radiation and water limitation, using the analytical expression of Ghausi et al. (2025). In the results, we evaluate this approach globally, then show the temporal and regional variations and the extent to which we capture observed VPD. We examine specifically the responses of VPD to variations to solar radiation and soil water limitation across geographic regions to link it back to the hump-shaped evaporation-VPD relationship. We close with a brief discussion, summary and conclusions.

https://doi.org/10.5194/egusphere-2026-3930
Preprint. Discussion started: 14 July 2026

2 Methodology and Data Sources

We start with the definition of the vapor pressure deficit, VPD, being the difference between the saturation, e_{sat}, and the actual vapor pressure, e_a, of air with a temperature T_a,

$$VPD = e_{sat} - e_a \tag{1}$$

Expressing the actual vapor pressure in terms of its dewpoint temperature, T_{dew}, with $e_a = e_{sat}(T_{dew})$, and using the derivative of the saturation vapor pressure curve, $s = de_{sat}/dT$, to linearize Eq. (1), we can express the VPD as

$$VPD = e_{sat}(T_a) - e_{sat}(T_{dew}) \approx s\ (T_a - T_{dew}) \tag{2}$$

The maximum value of VPD can then be related to the maximum of the air temperature, T_{max}, during the day, that is

$$VPD_{max} \approx s\ (T_{max} - T_{dew}) = s\ (T_{max} - T_{min}) + s\ (T_{min} - T_{dew}) \tag{3}$$

where T_{min} is the daily minimum air temperature. We then write VPD_{max} as

$$VPD_{max} = VPD_{min} + \Delta VPD \tag{4}$$

which is then related to the two temperature differences in Eq. (3),

$$VPD_{min} = s\ .\ (T_{min} - T_{dew}) \tag{5}$$

and

$$\Delta VPD = s\ (T_{max} - T_{min}) = s\ .\ DTR \tag{6}$$

where DTR is the diurnal temperature range, DTR = T_{max} - T_{min}. Since VPD_{min} is typically small or zero, the daily average of VPD is then dominated by the contribution of ΔVPD, which is then for a sinusoidal variation approximately given by $\mathrm{VPD}_{avg} \approx 2/\pi\ \Delta\mathrm{VPD} \approx \Delta\mathrm{VPD}/1.6$ (see Supp Fig. S1).

We then used an analytical expression for DTR developed in Ghausi et al. (2025), which links DTR to the radiative forcings and surface evaporative conditions. The expression is derived from an energy budget framework that accounts for i) surface energy balance, ii) heat storage changes within the boundary layer, which are fed by net exchange of longwave radiation

https://doi.org/10.5194/egusphere-2026-3930
Preprint. Discussion started: 14 July 2026

between the surface and the atmosphere as well as the sensible heat flux (Tian et al., 2023; McColl & Rigden, 2020), and iii) a thermodynamic constraint on turbulent exchange based on the maximum power limit (Kleidon & Renner 2013; Kleidon & Renner 2018; Ghausi et al., 2023). The maximum power limit sets the partitioning between net longwave radiation and turbulent fluxes, while the equilibrium partitioning sets the partitioning between the sensible and latent heat flux in the case of unconstrained evaporation. This combination results in an analytic expression for the DTR, which we rewrite here to highlight the two major drivers, absorbed solar radiation at the surface, R_s (in W m^{-2}), and a water availability factor, f_w (ranging from 0 to 1), defined as the ratio of actual to potential evaporation (Conte et al., 2019)

$$DTR = \frac{2\Delta t}{c_p \rho h} \cdot \left(\frac{2}{2 + f_w f_{eq}} R_s - \frac{f_w f_{eq}}{2 + f_w f_{eq}} \left(R_s + R_{l,d} - R_{l,toa} \right) \right) \tag{7}$$

where $R_{l,d}$ and $R_{l,toa}$ are the longwave radiative fluxes (in W m^{-2}), downward at the surface and outgoing at the top of the atmosphere respectively, f_{eq} is the equilibrium evaporative fraction (estimated using the equilibrium energy partitioning – details in Supp. text S1), c_p is the specific heat capacity of air (in J kg^{-1} m^{-3}), ρ is the air density (in kg m^{-3}), h is the daytime boundary layer height (in m, which is assumed to be constant and equal to 1000 m), and Δt is the length of daytime (i.e., $R_s >$ 0 in s). This expression shows how the DTR increases with absorbed solar radiation, the first term in the bracket, but is reduced by less-constrained evaporation through a greater value of f_w, the second term in the bracket.

When we combine the equation for ΔVPD (Eq. 6) and DTR (Eq. 7), we get an analytical expression that expresses the diurnal variation in VPD in terms of the main drivers: solar radiation and soil water stress. In the following, we evaluate the extent to which this approach can reproduce the observed values of VPD_{max} (Eq. 4), then decompose it into the parts driven by absorbed solar radiation, water stress, and VPD_{min}.

For this evaluation we use a combination of observationally derived global datasets. The analysis was performed using daily means over the period 2001-2018 and at a spatial grid resolution of 1°x1°. Daily radiative fluxes for the surface and top of atmosphere (R_s, $R_{l,d}$, $R_{l,toa}$) were obtained from NASA-CERES Syn1deg product (Doelling et al., 2013). Daily maximum and minimum temperatures (T_{min}, T_{max}, DTR) were taken from the CPC global daily temperature dataset. Daily dewpoint temperature (T_{dew}) was taken from ERA-5 (Hersbach et al., 2020). We used the GLEAM V3.6b dataset (Miralles et al., 2011; Martens et al., 2017) for actual evapotranspiration in order to infer values of water availability (factor f_w). Potential evapotranspiration was estimated using equilibrium partitioning (details in Supp. Text S1).

https://doi.org/10.5194/egusphere-2026-3930
Preprint. Discussion started: 14 July 2026

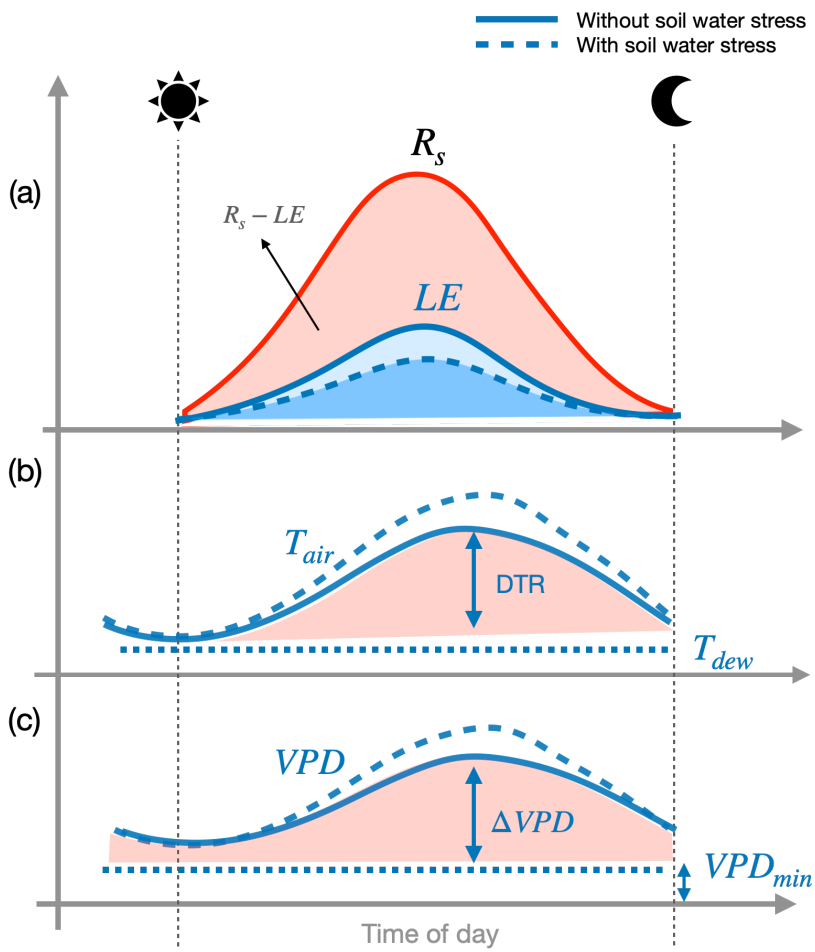

Figure 1: (A) Conceptual framework describing the link between absorbed solar radiation (R_s), evaporation (LE), diurnal air temperature range (DTR), and vapor pressure deficit (VPD). The top panel (a) shows the variation of R_s and LE during the day. The red shaded area represents the energy available for atmospheric heating ($R_s - LE$). The middle pane (b) shows the variation of resulting air temperature cycle T_{air}, the DTR as a result of atmospheric heating and the dewpoint temperature T_{dew}. The bottom panel (c) shows the corresponding VPD cycle, decomposed into a minimum value VPD_{min} and a daytime increase ΔVPD due to changes in T_{air}. The dashed blue curves represent a water-limited case with reduced evaporation, leading to greater atmospheric heating, a larger DTR, and a larger daytime increase in VPD than the wetter case shown by the solid blue curves.

https://doi.org/10.5194/egusphere-2026-3930
Preprint. Discussion started: 14 July 2026

3 Results and Discussion

To evaluate our expression for daily maximum VPD (Eq. 4), we computed ΔVPD using the expression for DTR (Eq. 8), using the radiative fluxes, soil water availability and added VPD_{min} derived from observations. Notably, more than 60% of daily observations globally have $VPD_{min} < 0.2$kPa, indicating that $T_{dew} \approx T_{min}$, in most cases; this fraction increases to about 80% in humid tropical regions and at high latitudes (Supp. Fig. S2). We then compared estimated VPD_{max} against observations derived using gridded maximum and minimum air temperatures and dew point temperatures. After this evaluation, we analyzed the role of soil water stress on VPD, quantified the relative importance of solar radiation and water stress across regions to then get back to the relationship between evaporation and VPD.

3.1 Estimating VPD from DTR

Fig. 2A, B show maps of mean annual estimated and observed VPD_{max}, while Fig. 2C presents the grid-point comparison of VPD_{max} estimates vs. observed values. Our expression captures observed VPD_{max} very well with slope of 0.92, R^2 of 0.91 and a root mean squared error (RMSE) of 0.34 kPa. The RMSE for each grid point remain less than 0.5 kPa across all data points (Supp Fig. S2).

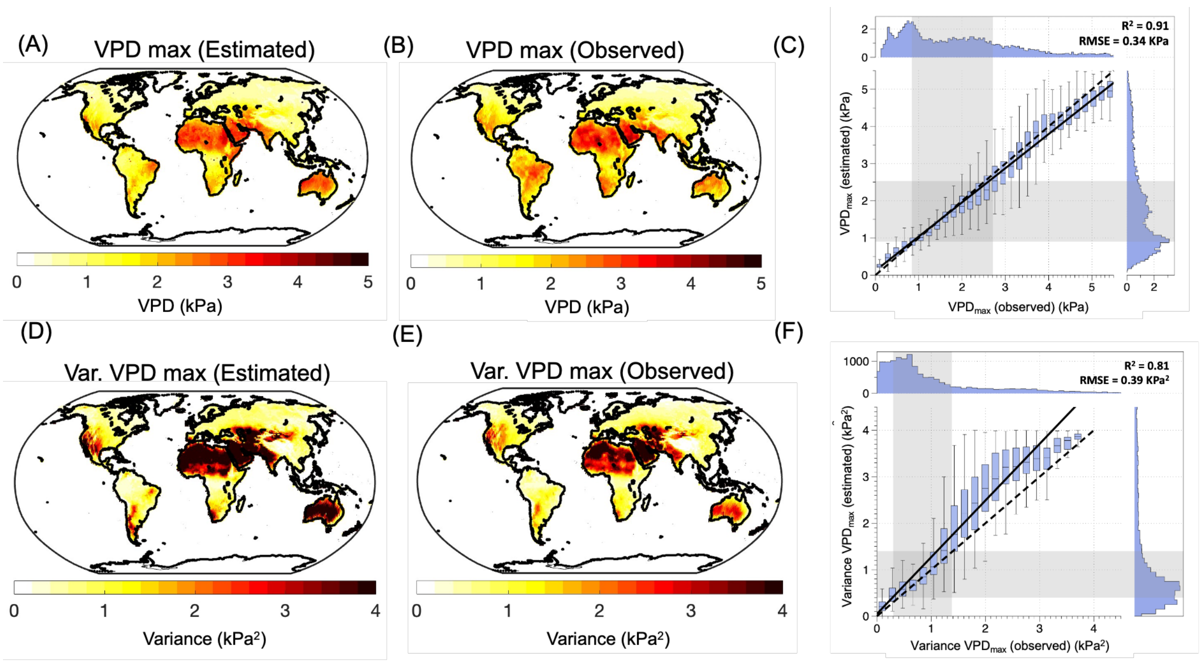

Figure 2: Global maps of the geographic variation in the (A) estimated and (B) observations of the mean annual daily maximum VPD. (D, E) same as (A, B) but for grid-point variance in daily maximum VPD. (C) Comparison of estimated and observed daily maximum VPD. (F) same as (C) but for grid-point variance.

https://doi.org/10.5194/egusphere-2026-3930
Preprint. Discussion started: 14 July 2026

Our expression also reproduces observed temporal variability at each grid point reasonably well. Fig. 1D, E shows the daily variance in VPDmax for estimated and observed values, respectively, and Fig. 1F shows the grid-point comparison. The expression explains both the magnitude and spatial structure of the variance well (slope = 1.21, $R^2 = 0.81$, RMSE = 0.39 kPa^2), although there is a slight systematic bias in overestimating this variance.

These comparisons show that our approach effectively captures both the spatial and temporal variation in daily maximum VPD. This implies that VPD_{max}, and, when averaged over the course of the day, the mean values of VPD, are primarily shaped by the heat input into the lower atmosphere during the day. The same reasoning applies to variations in relative humidity because VPD and relative humidity are directly connected to each other.

3.2 VPD response to soil water stress

We next examine the relative roles of solar radiation and soil water stress in shaping both, the DTR as well as the VPD. To do so, we constructed a two-dimensional phase space with soil water stress ($1 - f_w$) on the x-axis and solar radiation on the y-axis for observations as well as estimated by our approach (Fig. 3).

Observed DTR shows a systematic variation along both axes: for a given level of absorbed solar radiation (R_s), DTR increases with water stress ($1 - f_w$) by up to 6K, and for a given level of water stress, DTR increases with solar radiation by up to 10 K (Fig. 3A). This dependence is well reproduced by the analytical expression for DTR (Fig. 3B), confirming that the model captures how both, solar radiation and water limitation that shape variations in diurnal air temperatures (see also Eq. (7)).

We then evaluated whether this imprint on DTR translates directly into VPD. To do so, we compared observed diurnal variations in VPD ($\Delta VPD = VPD_{max} - VPD_{min}$) with values estimated using the (Eq. (6)). Observed ΔVPD exhibits the similar dependence on radiative heating and water stress as shown by DTR (Fig. 3C). For a fixed solar radiation, VPD increases by up to 2 kPa due to water stress. This behaviour is very well captured by our analytical estimate (Fig. 3D).

https://doi.org/10.5194/egusphere-2026-3930
Preprint. Discussion started: 14 July 2026

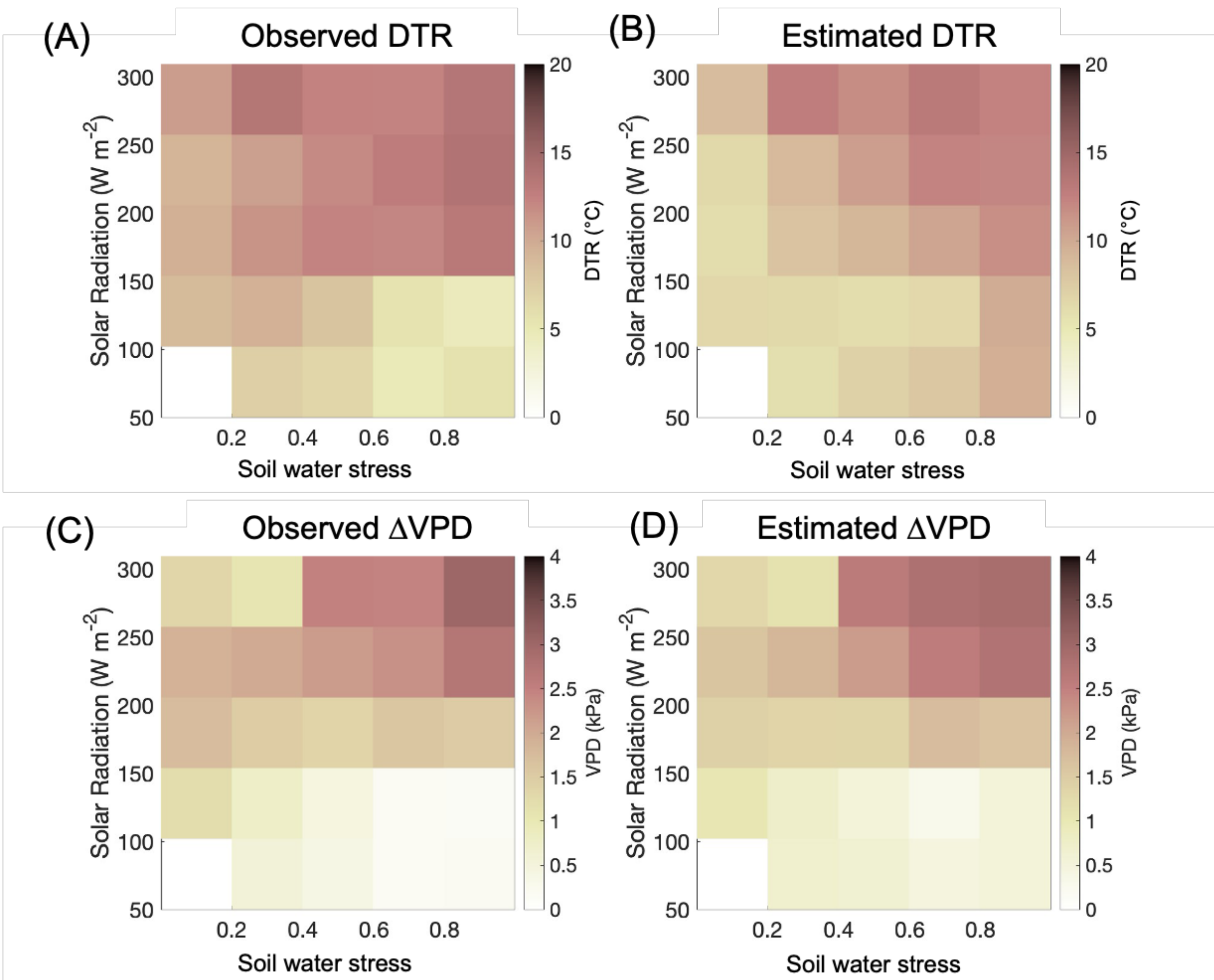

Figure 3: Variation of observed (A) and estimated(B) diurnal air temperature range (DTR) over the phase space defined by different soil water stress (f_{ws}) along the x-axis and solar radiation along the y-axis. (C, D) same as A, B but for observed and estimated diurnal changes in VPD respectively.

These results demonstrate that diurnal variations in VPD primarily reflect changes in atmospheric heating rather than changes in atmospheric moisture. In other words, VPD increases under high radiative forcing and water stress not because of direct changes in moisture supply, but because enhanced sensible heating drives larger diurnal temperature variations, which in turn elevates the saturation vapor pressure and amplifies the VPD.

https://doi.org/10.5194/egusphere-2026-3930
Preprint. Discussion started: 14 July 2026

3.3 Geographic distribution of VPD contributions

We next show how these two factors, solar radiation and water stress, explain the observed geographic patterns of the VPD. To do so, we use Eq. (4) and decompose VPD_{max} into three terms: (i) the direct contribution by solar radiative heating, (ii) the enhancement by soil water stress , and (iii) daily minimum VPD. The first term represents the diurnal increase in VPD due to air temperature changes driven by absorption of radiation at the surface. We calculate this contribution using Eq. (7) for DTR with $f_w = 1$ and then use Eq. (6) to calculate ΔVPD in the absence of soil water stress. The second contribution to VPD represents the additional diurnal increase caused by soil water stress, reduced evaporation and enhanced sensible heating of the lower atmosphere. This enhances the DTR, as can be seen by the second term in Eq. (7) for soil water stress, i.e., $f_w < 1$. To calculate this contribution, we compute the difference in DTR by calculating Eq. 7 for an idealized non-stressed surface ($f_w = 1$) and the actual value of f_w. We then use Eq. 6 to translate this into a contribution to ΔVPD. The contribution to VPD variations by VPD_{min} is taken directly from the dataset.

The geographic distribution of these three contributions to VPD are shown in Fig. 4. We note that radiation is by far the largest term, particularly in humid regions, contributing at least 50% to the VPD across latitudes. In desert regions, particularly over Northern Africa, the Arabian Peninsula and Australia, the contributions by soil water stress and VPD_{min} are both of similar magnitude and result in higher VPD values. There is also an unexplained contribution of less than 20% to VPD variations that is relatively independent of latitude. In combination, these contributions result in the well-documented, characteristic M-shaped zonal structure in VPD. The high values of VPD in the dry subtropics can thus be attributed to a large extent to high levels of solar radiation and water limitation, which are consequences of the descending branch of the tropical Hadley circulation.

https://doi.org/10.5194/egusphere-2026-3930
Preprint. Discussion started: 14 July 2026

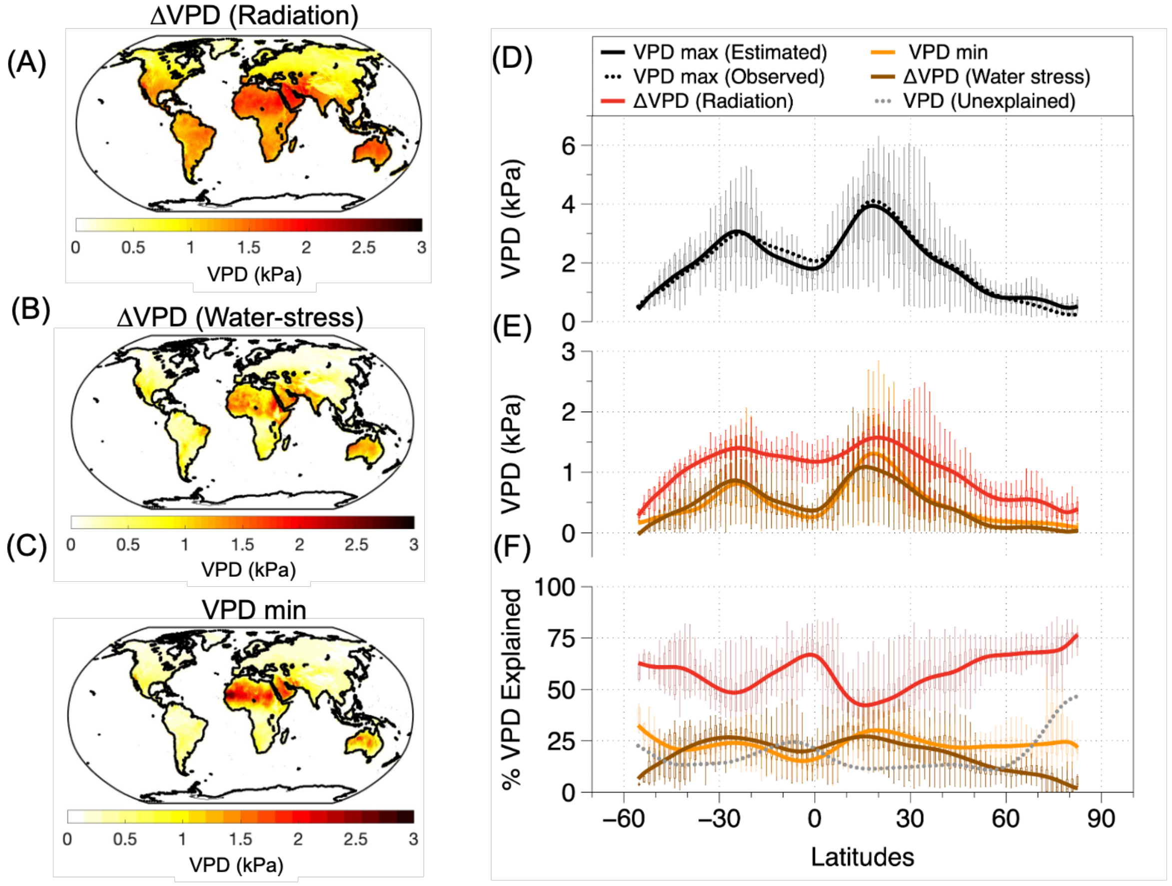

215 **Figure 4: (A-C) Global maps showing spatial distributions of (A) VPD due to radiation (ΔVPD Radiation), (B) VPD due to soil water-stress (ΔVPD Water-stress), and (C) the minimum VPD (VPD_min). (D) Zonal mean values of daily maximum VPD (observed and estimated) and its decomposed components plotted against latitude. (E) Zonal means of the three decomposed VPD components against latitude. (F) Percent of VPD explained by each component as a function of latitude. VPD values are in kPa.**

These results are also consistent with a recent theoretical work (McColl and Tang (2024)) which demonstrated that long-term zonal averages of near-surface relative humidity (RH) are diagnostically linked to the surface evaporative fraction. Our estimated contribution of surface water stress to VPD has an M shaped profile (Fig. 4D) which is consistent with the W shaped zonally average profile of RH caused by surface water limitation (McColl and Tang (2024)). This decomposition demonstrates that while radiative forcing exerts the dominant thermodynamic control on VPD globally, surface evaporative constraints and background atmospheric moisture act as modulators, particularly in arid and semi-arid regions.

https://doi.org/10.5194/egusphere-2026-3930
Preprint. Discussion started: 14 July 2026

3.4 VPD and Evaporation

Finally, we use our explanation for the dominant controls on VPD to re-examine the observed hump-shaped evaporation-VPD relationship (Massmann et al., 2019; Grossiord et al., 2020). To do so, we plot evaporation versus VPD in Fig. 5B. It shows the well-documented hump, in which evaporation first increases with VPD, reaches a maximum, but then declines beyond a certain range of VPD values. While this behavior is commonly attributed to plant physiological responses, such as stomatal closure under high VPD, we show that this relationship can also be explained by the transition between energy- and water-limited evaporative regimes (Koster et al., 2009; Seneviratne et al., 2010) and their effects on the diurnal temperature range (DTR), and thus on VPD. The observed relationship is well captured using both observed (red) and estimated (blue) VPD, indicating that the underlying controls are represented by our framework. Fig. 5B also shows that the radiative forcing no longer increases beyond the hump at a VPD value of about 2 kPa. Hence, the additional increase in VPD is not due to greater radiative heating, but rather due to the enhanced heating of the lower atmosphere due to soil water stress.

The link to our explanation of VPD is made by first noting that neither evaporation nor VPD are independent forcings of the land-atmosphere system. Both depend on solar radiation and soil water availability, which affect not just VPD, but also DTR so that we see the same effects in DTR. We therefore also plot evaporation and the DTR versus absorbed solar radiation R_s (Fig. 5C). In this plot, we note how evaporation increases with solar radiation (energy-limited conditions), levels off at around 150-200 W m^{-2}, beyond which it decreases due to soil water stress (water-limited conditions). In other words, it also shows a hump-shaped relationship when plotted against solar radiation. The effect of soil water stress is then reflected in an elevated DTR.

The hump-backed shape can then be explained as follows: Evaporation increases with absorbed solar radiation, R_s, because more energy is available to sustain the phase transition, but is reduced by soil water stress (i.e., the factor $1 - f_w$). These two dependencies can clearly be seen in Fig. 5C. The DTR also increases with absorbed solar radiation, because R_s is the main factor shaping the diurnal temperature range (see Eq. 7), which then shapes ΔVPD (Eq. 6). When soil water becomes limiting (small values of f_w), the lower atmosphere is heated more due to reduced evaporation, this enhances the DTR and hence, VPD. The hump-backed shape is then explained as follows: Since both, evaporation and VPD, depend primarily on absorbed solar radiation, they show initially a close linear relationship, up to the point when soil water stress starts to limit evaporation. Then, the reduced latent heat flux increases the DTR further. In our equations, this can be seen in Eq. 7, where the DTR increases for smaller f_w for given R_s. This then translates into higher values of VPD. The decreasing branch of the evaporation-VPD curve at high VPD values is thus caused by soil water stress. This provides an alternative pathway to get a hump-shaped

https://doi.org/10.5194/egusphere-2026-3930
Preprint. Discussion started: 14 July 2026

evaporation-VPD relationship solely based on the changes in lower atmospheric heating under water and energy limited conditions.

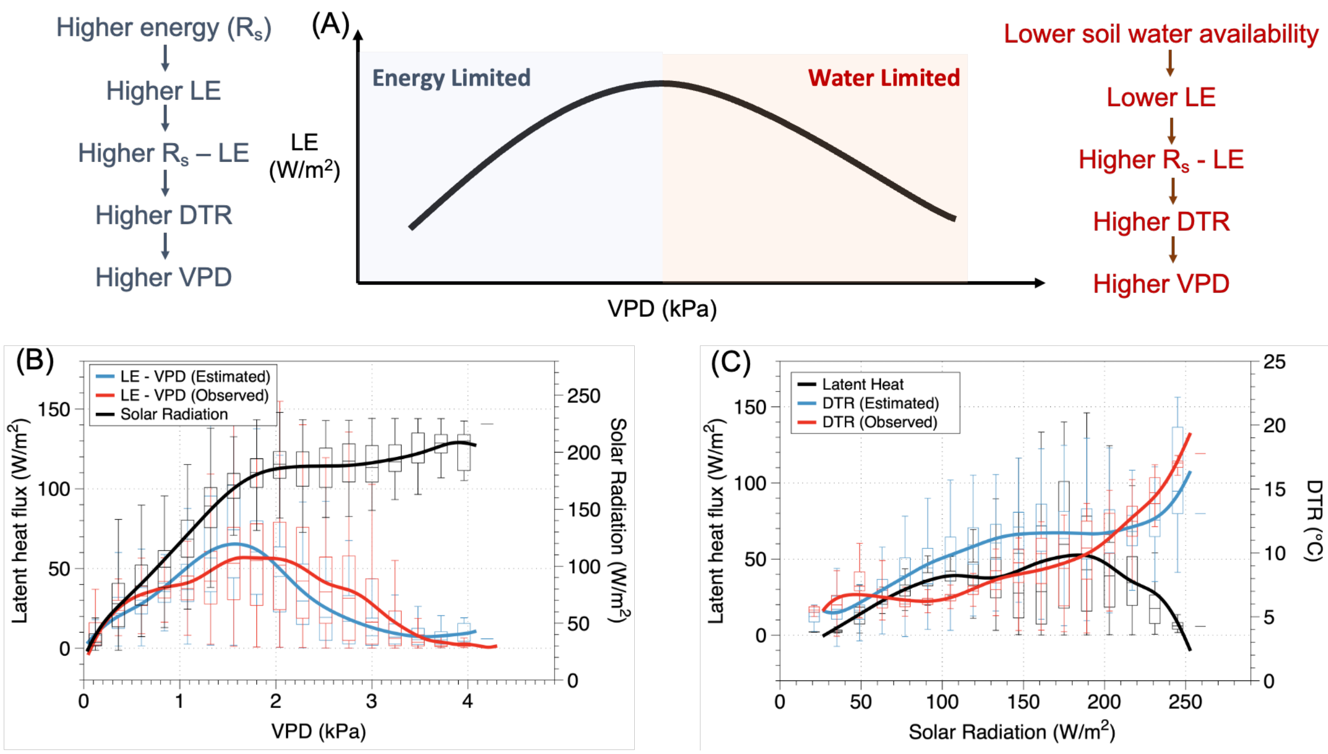

Figure 5: (A) Relationship between latent heat flux (LE) and vapor pressure deficit (VPD), showing the characteristic hump-shaped curve. Results are shown for LE vs VPD observed (in red) and LE vs VPD estimated in (blue), with absorbed solar radiation (black) increasing with VPD. (B) Latent heat flux variation with solar radiation (black), illustrating the transition from energy-limited to water-limited regimes, where declining LE increases the diurnal temperature range (DTR; observed in red, estimated in blue) that leads to higher VPD.

It is important to note that our results do not imply that vegetation is insensitive to VPD or that physiological responses to atmospheric dryness are unimportant. Numerous experimental and observational studies have demonstrated direct stomatal, hydraulic and productivity responses to increasing VPD (Novick et al., 2016; Grossiord et al., 2020; Yuan et al., 2019). Rather, our findings suggest that a substantial fraction of the observed variability in VPD itself can be understood as a consequence of the radiative and hydrological factors shaping lower atmospheric heating and that non-linear evaporation-VPD relationship

https://doi.org/10.5194/egusphere-2026-3930
Preprint. Discussion started: 14 July 2026

can emerge simply by how this heating changes under water and energy limited regimes. This interpretation is consistent with recent observations from forest microclimates that found that temperature-driven saturation vapor pressure explained most of the observed landscape-scale variability in VPD (Růžičková et al., 2025).

Our interpretation also complements recent work that questioned the causal interpretations of VPD–ecosystem relationships and emphasizing the confounding controls exerted by radiation and soil moisture leading to misinterpretation of land–atmosphere feedbacks (Vargas Zeppetello et al., 2023) and aridity trends (Zhou & Yu, 2025). Our approach provides a physical framework that can help in disentangling the effects of VPD from those of soil moisture by characterizing periods where VPD is governed by changes in radiation, soil-water stress and atmospheric moisture.

Our results also connect closely to the analytical framework of McColl and Tang (2024), who showed that large-scale variations in near-surface relative humidity can be understood as a consequence of surface evaporative conditions. Our framework highlights how the partitioning of surface energy controls lower-atmospheric heating, the diurnal temperature range, and consequently VPD. Both of these perspectives suggest that commonly used measures of atmospheric dryness - irrespective of whether expressed as relative humidity or VPD - are not independent forcings of the land–atmosphere system, but can emerge from underlying confounding controls exerted by surface energy partitioning and soil water availability.

4 Summary and Conclusion

In this work, we provide a simple physical explanation for the observed spatiotemporal variability in VPD. We show that the dominant source of VPD variability arises from the diurnal heating of the lower atmosphere**.** These heat storage changes in the lower atmosphere shape the diurnal air temperature range, and through the Clausius–Clapeyron relationship, this warming increases the saturation vapor pressure and thereby the daytime increase in VPD. We used an analytical expression for DTR derived from surface energy balance and thermodynamic constraints and demonstrate that this approach reproduces the observed spatial and temporal variations in VPD remarkably well across continents and climate regimes. While a contribution from the night-time background atmospheric dryness (represented by minimum VPD) remains important, particularly in arid regions, most of the daytime variability in VPD can be explained by thermodynamic heating of the lower atmosphere.

Our framework demonstrates that solar radiation, clouds, and soil water stress influence VPD variability primarily through their effects on surface energy partitioning and boundary-layer heating, rather than through direct changes in atmospheric moisture content. This interpretation provides a simple physical explanation for the characteristic hump-shaped evaporation–VPD relationship. Under energy-limited conditions, increasing solar radiation enhances both evaporation and DTR, producing

https://doi.org/10.5194/egusphere-2026-3930
Preprint. Discussion started: 14 July 2026

increasing VPD. As conditions transition to water limitation, reduced evaporation increases sensible heating of the lower atmosphere, further amplifying DTR and VPD while evaporation declines. Thus, the observed non-linear relationship emerges naturally from changes in lower-atmospheric heating across energy- and water-limited regimes.

These findings suggest that VPD should be interpreted not only as an atmospheric state variable affecting ecosystem processes, but as an emergent response of the coupled land–atmosphere system to surface energy partitioning. This perspective has important implications for interpreting land–atmosphere feedbacks, evaluating projections in droughts and atmospheric aridity under global warming, and developing physically consistent diagnostics of ecosystem water stress. Additionally, our work provides a basis for characterizing periods during which VPD variability is controlled primarily by radiative forcing or by soil water stress. Such a decomposition offers a physical pathway for disentangling the effects of atmospheric dryness from those of soil moisture and can help improve attribution of ecosystem responses and land–atmosphere feedbacks. It also offers a simple benchmark for evaluating whether land-surface and Earth system models reproduce the dominant physical controls on VPD variability.

Future work should focus on better understanding the processes controlling night-time atmospheric dryness, represented here by the minimum VPD, and on extending this framework to quantify the relative contributions of radiation and soil water stress for investigating drought mechanisms, interpreting ecosystem responses to atmospheric dryness, and improving aridity projections.

Code and data availability

All datasets used in this study are publicly available. Daily radiative fluxes were obtained from the NASA CERES SYN1deg data product, https://ceres.larc.nasa.gov/data/ , provided by NASA Langley Research Center, Atmospheric Science Data Center, 2021). Daily maximum and minimum air temperatures data from CPC Global Unified Temperature dataset was provided by the NOAA PSL, Boulder, Colorado, USA and is accessible from https://psl.noaa.gov/data/gridded/data.cpc.globaltemp.html. Dew point temperature data from ERA-5 reanalysis can be accessed using https://doi.org/10.24381/cds.adbb2d47. GLEAM actual evaporation data is accessible from https://www.gleam.eu/. No new data was generated in our study.

https://doi.org/10.5194/egusphere-2026-3930
Preprint. Discussion started: 14 July 2026

Author contributions

SAG prepared the manuscript with contributions from all co-authors. All authors contributed to the idea and development of the hypothesis. SAG conducted the formal analysis, and wrote the original draft of the manuscript with inputs from TC and AK. All authors contributed to the interpretation of the results.

Competing interests

Some authors are members of the editorial board of journal Earth System Dynamics. The authors declare that they have no other conflict of interest.

All maps in this manuscript were generated by the authors using MATLAB Mapping Toolbox built-in geographic boundary data. No third-party map images were reproduced or adapted.

https://doi.org/10.5194/egusphere-2026-3930
Preprint. Discussion started: 14 July 2026

References

1. Allen, R. G., Pereira, L. S., Raes, D., & Smith, M.: Crop evapotranspiration – Guidelines for computing crop water requirements (FAO), 1998.

2. Gentine, P., Green, J. K., Guérin, M., Humphrey, V., Seneviratne, S. I., Zhang, Y., & Zhou, S.: Coupling between the terrestrial carbon and water cycles—a review. Environmental Research Letters, 14, 083003. DOI: 10.1088/1748-9326/ab22d6, 2019.

3. Yuan, W. et al.: Increased atmospheric vapor pressure deficit reduces global vegetation growth. Science Advances, 5, eaax1396. DOI: https://doi.org/10.1126/sciadv.aax1396, 2019.

4. Zhong, Z., He, B., Wang, Y. P., Chen, H. W., Chen, D., Fu, Y. H., Chen, Y., Guo, L., Deng, Y., Huang, L., & Yuan, W.: Disentangling the effects of vapor pressure deficit on northern terrestrial vegetation productivity. Science Advances, 9, eadf3166. DOI: https://doi.org/10.1126/sciadv.adf3166, 2023.

5. Franks, P. J., Cowan, I. R., & Farquhar, G. D.: The apparent feedforward response of stomata to air vapour pressure deficit: information revealed by different experimental procedures with two rainforest trees. Plant, Cell & Environment, 20(1), 142-145, https://doi.org/10.1046/j.1365-3040.1997.d01-14.x, 1997.

6. Medlyn, B. E., Duursma, R. A., Eamus, D., Ellsworth, D. S., Prentice, I. C., Barton, C. V., ... & Wingate, L.: Reconciling the optimal and empirical approaches to modelling stomatal conductance. Global change biology, 17(6), 2134-2144, https://doi.org/10.1111/j.1365-2486.2010.02375.x, 2011.

7. Grossiord, C., Buckley, T. N., Cernusak, L. A., Novick, K. A., Poulter, B., Siegwolf, R. T., Sperry, J. S., & McDowell, N. G.: Plant responses to rising vapor pressure deficit. New Phytologist, 226, 1550-1566. DOI: 10.1111/nph.16485, 2020.

8. Sherwood, S., & Fu, Q.: A drier future?. Science, 343(6172), 737-739. DOI:10.1126/science.1247620, 2014.

9. Novick, K. A., Ficklin, D. L., Grossiord, C., Konings, A. G., Martínez-Vilalta, J., Sadok, W., Trugman, A. T., Williams, A. P., Wright, A. J., Abatzoglou, J. T., & Dannenberg, M. P.: The impacts of rising vapour pressure deficit in natural and managed ecosystems. Plant, Cell & Environment, 47, 3561-3589. DOI: 10.1111/pce.14846, 2024.

10. Zhang, S., Wang, W., Wei, J., Qian, H., Wamucii, C. N., & Teuling, A. J.: Land-atmosphere interaction during heat waves diagnosed using vapor pressure deficit dynamics. Journal of Hydrology, 645, 132181. DOI: https://doi.org/10.1016/j.jhydrol.2024.132181, 2024.

11. Fang, Z., Zhang, W., Brandt, M., Abdi, A. M., & Fensholt, R.: Globally increasing atmospheric aridity over the 21st century. Earth's Future, 10, e2022EF003019. DOI: https://doi.org/10.1029/2022EF003019, 2022.

12. Zhou, S., & Yu, B.: Neglecting land–atmosphere feedbacks overestimates climate-driven increases in evapotranspiration. Nature Climate Change, 15, 1099-1106. DOI: https://doi.org/10.1038/s41558-025-02428-5, 2025.

13. Huang, J., Yu, H., Guan, X., Wang, G., & Guo, R.: Accelerated dryland expansion under climate change. Nature Climate Change, 6, 166-171. DOI: 10.1038/nclimate2837, 2016.

14. Berg, A., & McColl, K. A.: No projected global drylands expansion under greenhouse warming. Nature Climate Change, 11, 331-337. DOI: 10.1038/s41558-021-01007-8, 2021.

15. Liu, L., Gudmundsson, L., Hauser, M., et al.: Soil moisture dominates dryness stress on ecosystem production globally. Nature Communications, 11, 4892. DOI: https://doi.org/10.1038/s41467-020-18631-1, 2020.

16. Lu, H., Qin, Z., Lin, S., et al.: Large influence of atmospheric vapor pressure deficit on ecosystem production efficiency. Nature Communications, 13, 1653. DOI: https://doi.org/10.1038/s41467-022-29009-w, 2022.

17. Fu, Z., Ciais, P., Prentice, I.C. et al.: Atmospheric dryness reduces photosynthesis along a large range of soil water deficits. Nat Commun 13, 989). https://doi.org/10.1038/s41467-022-28652-7, 2022.

18. Novick, K., et al.: The increasing importance of atmospheric demand for ecosystem water and carbon fluxes. Nature Climate Change, 6, 1023-1027. DOI: 10.1038/nclimate3114, 2016.

19. Buckley, T. N.: How do stomata respond to water status?. New Phytologist, 224(1), 21-36. https://doi.org/10.1111/nph.15899, 2019.

https://doi.org/10.5194/egusphere-2026-3930
Preprint. Discussion started: 14 July 2026

20. Vargas Zeppetello, L. R., McColl, K. A., Bernau, J. A., et al.: Apparent surface conductance sensitivity to vapour pressure deficit in the absence of plants. Nature Water, 1, 941-951. DOI: https://doi.org/10.1038/s44221-023-00147-9, 2023.

21. Tian, Y., Zhong, D., Ghausi, S. A., Wang, G., & Kleidon, A.: Understanding variations in downwelling longwave radiation using Brutsaert's equation. Earth System Dynamics, 14(6), 1363-1374, 2023.

22. McColl, K. A., & Rigden, A. J.: Emergent simplicity of continental evapotranspiration. Geophysical Research Letters, 47(6). https://doi.org/10.1029/2020GL087101, 2020.

23. Ghausi, S. A., McColl, K., Zehe, E., & Kleidon, A.: Explaining observed daily variations and decadal trends in the diurnal air temperature range. Geophysical Research Letters, 52, e2024GL113595. DOI: https://doi.org/10.1029/2024GL113595, 2025.

24. Zhang, Q., Manzoni, S., Katul, G., Porporato, A., & Yang, D.: The hysteretic evapotranspiration—Vapor pressure deficit relation. Journal of Geophysical Research: Biogeosciences, 119(2), 125-140. https://doi.org/10.1002/2013JG002484, 2014.

25. Massmann, A., Gentine, P., & Lin, C.: When does vapor pressure deficit drive or reduce evapotranspiration? Journal of Advances in Modeling Earth Systems, 11, 3305-3320. DOI: 10.1029/2019MS001790, 2019.

26. Kleidon, A., and M. Renner: Thermodynamic limits of hydrologic cycling within the Earth system: Concepts, estimates, and implications, Hydrology and Earth System Science, 17(7), 2873– 2892, DOI:10.5194/hess-17-2873-2013, 2013.

27. Kleidon, A. and Renner, M.: Diurnal land surface energy balance partitioning estimated from the thermodynamic limit of a cold heat engine, Earth Syst. Dynam., 9, 1127–1140, https://doi.org/10.5194/esd-9-1127-2018, 2018.

28. Ghausi, S. A., Tian, Y., Zehe, E., & Kleidon, A.: Radiative controls by clouds and thermodynamics shape surface temperatures and turbulent fluxes over land. Proceedings of the National Academy of Sciences, 120, e2220400120. DOI: https://doi.org/10.1073/pnas.2220400120, 2023.

29. Conte, L., Renner, M., Brando, P., Oliveira dos Santos, C., Silvério, D., Kolle, O., Trumbore, S.E. and Kleidon, A.: Effects of tropical deforestation on surface energy balance partitioning in southeastern Amazonia estimated from maximum convective power. Geophysical Research Letters, 46(8), pp.4396-4403 https://doi.org/10.1029/2018GL081625, 2019.

30. Doelling, D. R., et al.: Geostationary Enhanced Temporal Interpolation for CERES Flux Products. Journal of Atmospheric and Oceanic Technology, 30, 1072-1090. DOI: 10.1175/JTECH-D-12-00136.1, 2013.

31. Hersbach, H., et al.: The ERA5 global reanalysis. Quarterly Journal of the Royal Meteorological Society, 146, 1999-2049. DOI: https://doi.org/10.1002/qj.3803, 2020.

32. Miralles, D. G., Holmes, T. R. H., De Jeu, R. A. M., Gash, J. H., Meesters, A. G. C. A., & Dolman, A. J.: Global land-surface evaporation estimated from satellite-based observations. Hydrology and Earth System Sciences, 15, 453-469. DOI: https://doi.org/10.5194/hess-15-453-2011, 2011.

33. Martens, B., Miralles, D. G., Lievens, H., van der Schalie, R., de Juego, R. A. M., Fernández-Prieto, D., Beck, H. E., Dorigo, W. A., & Verhoest, N. E. C.: GLEAM v3: satellite-based land evaporation and root-zone soil moisture. Geoscientific Model Development, 10, 1903-1925. DOI: https://doi.org/10.5194/gmd-10-1903-2017, 2017.

34. McColl, K. A. & Tang L.: An Analytic Theory of Near-Surface Relative Humidity over Land. J. Clim. 37, 1213–1230 (2024). https://doi.org/10.1175/JCLI-D-23-0342.1, 2024.

35. Růžičková, A., Man, M., Macek, M., Wild, J., and Kopecký, M.: Temperature-driven vapor pressure deficit structures forest bryophyte communities across the landscape, Biogeosciences, 22, 6291–6307, https://doi.org/10.5194/bg-22-6291-2025, 2025.

36. Koster, R.D., Wang, H., Schubert, S.D., Suarez, M.J. and Mahanama, S.: Drought-induced warming in the continental United States under different SST regimes. Journal of Climate, 22(20), pp.5385-5400. https://doi.org/10.1175/2009JCLI3075.1, 2009.

https://doi.org/10.5194/egusphere-2026-3930
Preprint. Discussion started: 14 July 2026

37. Seneviratne, S. I., Corti, T., Davin, E. L., Hirschi, M., Jaeger, E. B., Lehner, I., Orlowsky, B., and Teuling, A. J.: Investigating soil moisture-climate interactions in a changing climate: A review, Earth-Sci. Rev., 99, 125–161, https://doi.org/10.1016/j.earscirev.2010.02.004, 2010.